Geoinformation for European-wide Integration, Benes (ed.)

Aliasing assessment and mitigation of PRISM hyperspectral sensor simulated images

B. Aiazzi, S. Baronti & L. Santurri
Institute of Applied Physics "Nello Carrara" IFAC-CNR, Firenze, Italy

A. Capanni
Galileo Avionica, Campi Bisenzio, Firenze, Italy

R. Vitulli
Vitrociset Netherlands, c/o ESA ESTEC, TOS/ETD, Noordwijk, Netherlands

Keywords: multispectral images, aliasing, digital filtering, restoration

ABSTRACT: The paper proposes a procedure to assess the aliasing effects that may produce distortions on remote sensing images acquired by hyper-spectral push-broom sensors and that arise because of sampling. Real images recorded over different targets at a resolution that is high for the sensor under investigation are used for the analysis. A model for the system modulation transfer function of PRISM hyper-spectral push-broom sensor is developed by taking into account the different contributions due to optical layout, electronics, detector, satellite motion. By using the sensor model, the high resolution images are pre-filtered and spatially re-sampled in order to obtain simulated images of the sensor. Such images are compared with those obtained by an *ideal* pre-filtering and re-sampling process in order to evidence possible aliasing effects. Quantitative indexes are adopted to assess the presence of aliasing. Digital filtering is adopted to mitigate aliasing effects; to this aim a multi-resolution filter and a fuzzy filter are evaluated. Quantitative and qualitative results show that the proposed filters are effective in aliasing mitigation with negligible penalties on spatial resolution.

1 INTRODUCTION

This work reports about the project realized under the ESA contract "*Study on Coupling Radiometry-Image Quality for Hyperspectral Applications*", undertaken by Galileo Avionica and IFAC-CNR. The objectives of the project were to assess the presence of aliasing in images to be acquired by PRISM hyper-spectral push-broom sensor and to experiment filtering algorithms to process such images after the acquisition process in order to mitigate aliasing effects.

PRISM instrument acquires images that are co-registered with high-accuracy in all spectral bands so that a same scene image acquisition provides a set of so-called spectral images. In the region 1 (from 450 nm to 2.35 μm) the imager has an high spectral resolution (10 to 15 nm) and a high number of bands (144). PRISM is a push-broom imaging spectrometer and a TIR imager (ESA ESTEC 1999): in the across track direction the image size is defined by the instantaneous filed of view while the Spatial Sampling Interval (SSI) is determined by the detector pitch; in the along track direction the image size is defined by the acquisition time and the SSI is determined by the integration time on a single pixel. Due to the orbital parameters the SSI is about 50m in both across and along track direction. A de-pointing mirror provides a ± 35° accessibility in the across track direction. A TMA telescope (Diameter of about 100 mm and f/4) collects the radiation from the useful spectral range in an intermediate image where a slit is located. In this image, the optical path of the TIR is separated in field by reflection in the direction of the velocity and the region 1 path enters in the spectrometer which disperses the light in the spectral direction and separates spectrally the VNIR (Visible Near InfraRed) and SWIR (Short Wave InfraRed) paths to direct them on 2D focal planes. The spectral direction is the along track direction, thus the ground projection of the spectrometer slit is across track. At the detector the input image is digitised.

When an analogue signal is digitalized, an insufficient sampling rate can cause the introduction of unwanted effects in the samples of the signal: the aliasing phenomenon (Oppenheim & Shafer 1989, Pratt 1978). For images this phenomenon is visible when samples are used to produce a reconstructed image; aliasing generates artefacts that degrade the visual quality of the reconstruction (Vollmerhausen 1999, 2000). Unfortunately, visual degradation is only one of the effects; any processing occurring on

the digital samples is applied on an *aliased* signal and thus may not produce the wanted result.

Nyquist's (Nyquist 1928) and Shannon's work (Shannon 1949) demonstrated that a band-limited signal can be exactly reconstructed by its samples if the sampling frequency is equal or greater than two times the maximum frequency of the original signal. Let us represent an image as a function $g(x,y)$ and denoted as ξ_{MAX}, η_{MAX} the maximum spatial frequencies of the signal to be sampled along the x and y spatial directions. In the practice, this image can be considered as band-limited because of the pre-filtering of the optical system that determines a cut-off on the Fourier spectrum of the input signal. Therefore ξ_{MAX}, η_{MAX} will denote the minimum value between the corresponding cut-off frequency and the maximum value of the spatial frequency of the original analogue image along x and y direction, respectively. In the practice, the original signal will not be band-limited and thus ξ_{MAX} and η_{MAX} will be determined by the optical system. If we denote with f_s^x and f_s^y the sampling frequencies along x and y, respectively and with ΔX, ΔY the spatial sampling step, the sampling theorem states that perfect reconstruction of an image from its samples is possible when

$$\left(\frac{1}{\Delta X}\right) = f_s^x \geq 2\xi_{MAX} \ , \qquad \left(\frac{1}{\Delta Y}\right) = f_s^y \geq 2\eta_{MAX}$$

The effect of sampling in the Fourier frequency domain is to originate replicas of the spectrum of $g(x,y)$ at any integer multiple of f_s^x and f_s^y (Oppenheim & Shafer 1989, Pratt 1978) (spurious response). If Shannon's theorem hypotheses are not verified, the replicas overlap, causing the aliasing phenomenon; perfect reconstruction will be no longer possible. In particular, at least the one-order replicas of the spurious response will overlap the base-band response.

In the following the approach proposed to assess aliasing is presented. Some of the quantitative quality indexes that have been adopted are then defined. Afterwards the sensor model is presented and discussed before its application to the selected test images. Aliasing is then assessed before and after restoration filtering. Visual results on some of the most significant tests are also presented and discussed.

2 THE PROPOSED APPROACH

Our approach was to analyze and assess the aliasing effects generated in the PRISM simulated images by comparing such images with those produced by an *ideal* sensor, i.e. a sensor that guarantees the maximum spatial nominal resolution (the same SSI of PRISM) without aliasing distortion. PRISM images can be produced by convolving the spatial response (SR) of the sensor with a proper set of test images thus. The test images should be characterized by an infinite spatial resolution thus determining an infinite extension of the Fourier spectrum. In the practice we can assume that an image is *a good test* when its spatial resolution is sufficiently higher than the resolution of the image to be simulated; in our experience, also supported by literature (Park & Rahman 1999, Jacobs & Edwards 1999) a factor of *4* is enough. Indeed, such a simple condition does not guarantee that every high resolution image is representative to evaluate aliasing when it is down-sampled by *4*. A good *ideal* test image should contain important spatial changes thus generating a significantly wide Fourier spectrum. In fact, if the test image is smooth, its spectrum will be narrow. Since aliasing is produced when, due to sampling, the replicas of Fourier's spectra overlap each other, maybe aliasing is not significant or absent for a smooth image.

Starting from the above considerations and taking into account that the SSI of PRISM is 50m, SPOT sensor panchromatic (PAN) images with an SSI of 10m can be considered as good test images for the PRISM sensor. SPOT images were thus adopted in our study as the primary test source to assess the aliasing effects of PRISM. Since aliasing is a signal dependent phenomenon it was convenient to adopt several test images characterized by different spatial frequency content and by significant spatial features whose distortions can be easily evidenced or measured by means of visual inspection or by using a convenient set of quantitative indexes as those reported in next chapter. Once the presence of aliasing is quantified some procedure to mitigate its effects can be adopted.

3 QUALITY INDEXES

Let be $G(\xi,\eta)$ the Fourier transform of $g(x,y)$. If an ideal reconstruction is adopted (by means of an ideal low pass filter) the definition of the In-band Spurious Response Ratio SR_{in} can be written in the following way:

$$SR = \frac{\int_{-\frac{1}{2\Delta Y}}^{\frac{1}{2\Delta Y}} \int_{-\frac{1}{2\Delta X}}^{\frac{1}{2\Delta X}} \left| \sum_{m=-\infty, m\neq 0}^{\infty} \sum_{n=-\infty, n\neq 0}^{\infty} |G|^2 \left(\xi + \frac{m}{\Delta X}, \eta + \frac{n}{\Delta Y} \right) \right|^{\frac{1}{2}} d\xi d\eta}{\int_{-\frac{1}{2\Delta Y}}^{\frac{1}{2\Delta Y}} \int_{-\frac{1}{2\Delta X}}^{\frac{1}{2\Delta X}} |G(\xi,\eta)| d\xi d\eta}$$

SR_{in} takes into account the energy of the spurious response falling inside the *base-band* and the energy

of *base-band response*. Since its value is usually low its percentage value will be reported.

An other method for evaluating aliasing in the spatial domain can be carried out by considering the inverse-transform $g_{SR}(x,y)$ of the spurious response $G_{SR}(\xi,\eta)$ (the last found as the difference between the Fourier transform of the aliased image and the base-band response); $g_{SR}(x,y)$ is in fact the spatial representation of artifacts related to aliasing effects. The artifacts can also be directly obtained by subtracting the *aliasing free* and the *aliased* image in the spatial domain. On $g_{SR}(x,y)$ visual judgements and quantitative measurements can be performed. Qualitative observations are performed by directly observing the image interpolated from $g_{SR}(x,y)$, while quantitative measurement can be performed by considering some measurements defined on $g_{SR}(x,y)$. The last measurements can be performed both in a local and/or in a global way, by evaluating the artifacts with an integration that spans on an area of interest or on the whole image respectively. In the project the peak error (PE) and the unchanged pixels percentage (UPP) were adopted. The former is the maximum absolute value on $g_{SR}(x,y)$ and has been adopted as a local quality index since it guarantees that at any pixel the error is lower than PE:

$$PE = \mathrm{Max}\,|\,g_{SR}(x,y)\,|\,\forall\, x,y$$

The latter represents the percentage of pixels that do not change between the *aliased* and *not-aliased* images. However, in order to prevent from noise problems, pixels that do not change are defined as those whose absolute value is equal or lower than *1*.

In the practice all the indexes that have been defined on analog images are measured on the corresponding sampled images i.e. on the matrix of samples in the spatial or in the transformed domain.

4 SPATIAL RESPONSE MODEL

The image forming process must take into account for loss of image fidelity as a function of spatial frequency or spatial resolution (Goodman 1996, Cooke et al. 1996). This degradation in fidelity is due to the overall degradation of the single sub-systems and can be quantified by either a sub-system Transfer Function (TF), for instance, the Optical Transfer Function (OTF) for the optical term, or by a spatial response, as the Point Spread Function (PSF) for the optical system. The final image captured by the system is obtained by taking the convolution of the system SR with the original input image or multiplying the system TF by the Fourier Transform of the original input image and then inverse Fourier transforming (IFT) this product. Assuming separability in the spatial frequency domain of the complex system Transfer Function, $TF_{SYS}(\xi,\eta)$ can be written as:

$$TF_{SYS}(\xi,\eta) = TF_{SYS}(\xi)TF_{SYS}(\eta)$$

This hypothesis implies also separability in the spatial domain, with the advantage that a more simple model of the instrument results. The approximation impact depends on the instrument characteristics. The other sub-system terms are spatially separable.

$$SR_{SYS}(x,y) = SR_{Across}(x)SR_{Along}(y)$$

An MTF (Modulation Transfer Function) cascade model is proposed for all terms, with an exception for the optical term in the across track direction, that is computed in the spatial domain: it is thus possible to maintain some information on the asymmetries due to the aberrations of the optical system.

$$SR_{Across}(x) = LSF_{Opt}(x) \otimes IFT\left[MTF_{Det}(\xi)\right]$$

Within the validity of the approximation of the PSF cross sections:

$$SR_{Across}(x) = PSF_{Opt}(x) \otimes IFT\left[MTF_{Det}(\xi)\right]$$

$$SR_{Along}(y) = IFT\left[MTF_{Diff}(\eta)MTF_{Win}(\eta)MTF_{Int}(\eta)\right]$$

SR across track is composed of the optical term, that takes into account of the overall optical system, and of the detector spatial response. Along track the instrument behaves as scanner instead as an imager.

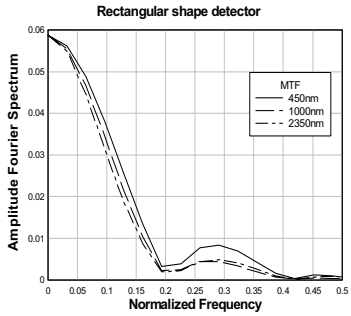

Figure 1. MTF across-track

For what concerns the transfer function of the optical system, given the high image quality of thetelescope, only the spectrometer transfer function can be considered with good approximation.

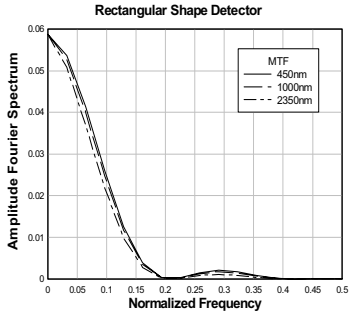

Figure 2. MTF along-track

Furthermore the transfer function, or in other terms the image quality, in the along track direction has no great impact on the overall transfer function, but only on the image intensity. Therefore, in terms of pure transfer function, this component seems to be negligible. In principle, known the object irradiance, it's possible to co-relate the image quality with the level of the signal from a detector pixel, stating the discrimination capability of the detector itself on the basis of its noise characteristics.

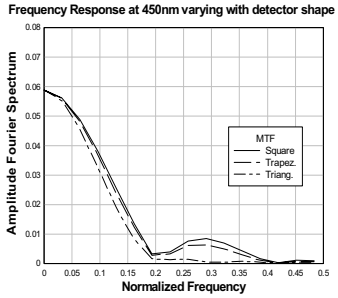

Figure 3. MTF across-track for three detector profiles

Figs. 1 and 2 report as examples the MTFs in the across and along track direction respectively, computed for three different wavelengths. A detector with rectangular uniform sensitivity profile has been assumed. In fact such a detector is the most critic for aliasing as shown in Fig. 3 for the across-track.

5 SIMULATED IMAGES

Six SPOT panchromatic (PAN) images were chosen as test set according to what discussed in section 2. Their SSI is 10m and the radiometric resolution is 8 bit. Each image has been pre-filtered with several MTFs, as those shown in Fig. 2, which have been obtained varying such system parameters as wavelengtht and sensor element shape. As an example of pre-filtering the result for Livorno test image (Fig. 4a) is shown for a wavelength of 450nm and a rectangular shape detector (Fig. 4b). The effect of prefiltering is apparent in Figs. 5a and 5b where the amplitude Fourier spectrum (AFS) of the images of Figs. 4a and 4b is reported, respectively. The AFSs have been streched to the same extent in order to evidence the presence of frequency components of order greater than 0.1. In fact, this normalized frequency represents the cut-off needed to avoid aliasing when a decimation factor of *5* is applied. Also the effect of the *ripple* of the filters of Figs. 1 and 2 is apparent.

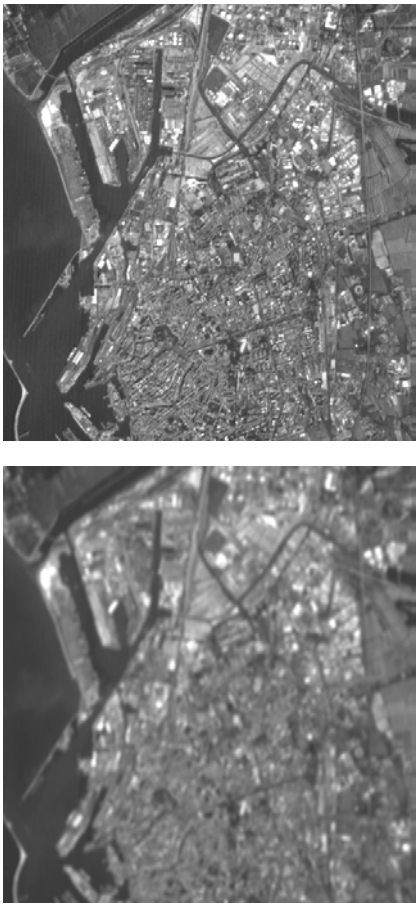

Figure 4. (a-top) Livorno test image: (b-bottom) Livorno prefiltered by instrument model at 450nm

Figs. 6a and 7a show the aliased images for Livorno and Pisa Airport test images, i.e. the images that have been decimated by a factor *5* (as in Fig. 4b) and successively interpolated by means of a *1/5* band interpolator for comparison purpose. Aliasing effects are present but hardly visible. Aliasiang appears, instead, in Figs. 6b and 7b that are the stre-

ched differences between the images of Fig. 6a, 7a and the *not aliased* images, respectively, that are obtained by properly filtering the images (as in Fig. 4b): a *near-ideal 1/5 band low-pass* filter is applied before the decimation-interpolation process. Aliasing is apparent on urban areas and on contours and linear features while is absent on homogeneous areas. This is due to the pre-filtering that does not completely prevent aliasing but is sufficient to limit the phenomenon to high frequency components.

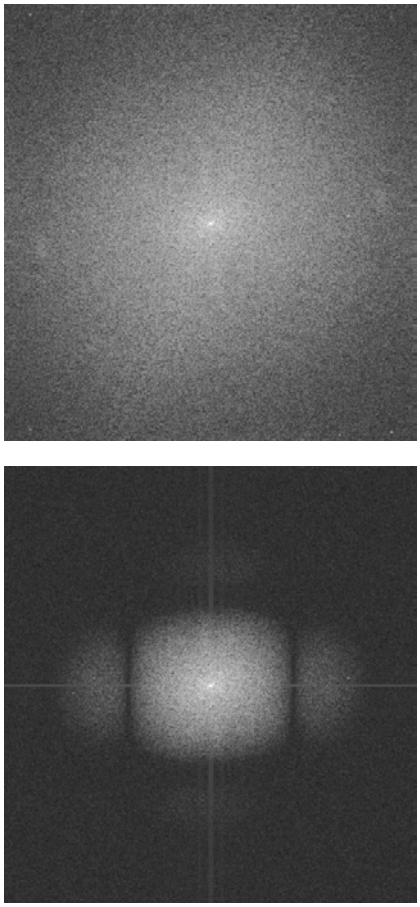

Figure 5. (a-top) AFS of Livorno; (b-bottom) AFS of Livorno after pre-filtering

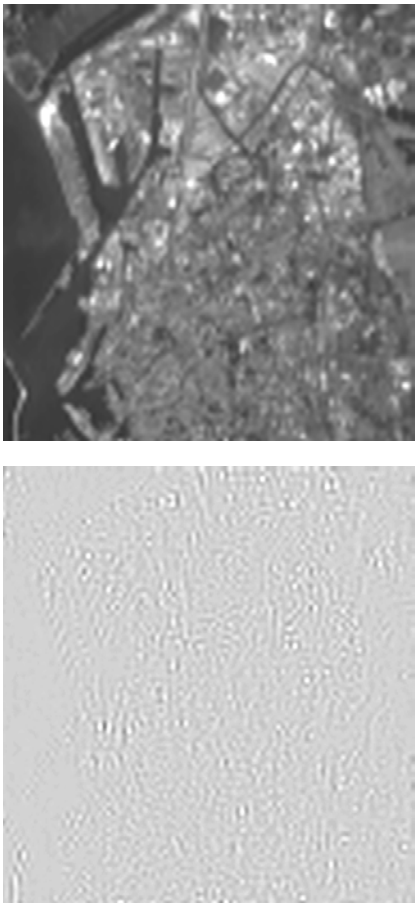

Figure 6. (a-top) Image 4a decimated and interpolated by 5; (b-bottom) difference between image 6a and *not-aliased* image

Table 1. Aliasing indices for Livorno image, prefiltered with the SR at 450 nm. The detector is assumed ideal with uniform sensitivity zones of 30µm , 20µm and 10µm respectively.

Livorno		Srin%	PE	UPP%
Uniform Detector Sensitiv. Width	30 µm	0.86	25	62.82
	20 µm	0.75	25	64.45
	10 µm	0.57	22	70.40

Table 2**.** Score indexes for Livorno image, prefiltered with instrument response at 450nm , 1000 nm, 2350 nm.

Livorno	Srin%	PE	UPP%
450 nm	0.86	25	62.82
1000 nm	0.62	19	68.59
2350 nm	0.47	16	74.39

6 ALIASING ASSESSMENT

Following the example of section 5, the simulation has been applied on all the test images. The tables that follow report the values of the score indexes introduced in section 2, computed when varying system parameters. Notice that all the indexes show a coherent behavior. UPP and PE are low when the aliasing is scarce while, conversely, UPP is high.

Table 1 refers to variation of sensor shape. Livorno image was chosen since it refers to an urban area and it was supposed to be a good test as confirmed by Table 3. Wavelength of 450nm was chosen because, as it can be deduced from Fig. 2 and it is clearly apparent in Table 2, aliasing effects are greater at this wavelength. The rectangular shape detector is the worst, as expected. When the sensitivity profile changes and becomes trapezoidal, aliasing decreases because the MTF becomes flatter in the *stop-band* (see again Fig.3).

Table 2 shows, as expected from Figs. 1 and 2, that aliasing decreases when wavelength increases. All next tables refer to a wavelength of 450 nm and ideal (30 μm width) detector element.

Table 3 shows the results for all the test images. Aliasing is high when a significant amount of linear features and edges is present (Livorno, Pisa airport), while, conversely, is low when large homogeneous areas appear in the test images (San Rossore). Concerning this point notice the behaviour of UPP parameter on San Rossore.

Table 3: Figures of merit of aliasing for the set of six test images, prefiltered at 450nm.

Test images	Srin%	PE	UPP%
Livorno	0.86	25	62.82
San Rossore	0.31	15	91.40
Pisa airport	0.91	21	69.32
Tuscany 1	0.41	19	83.24
Basilicata 1	0.40	25	73.29
Basilicata 2	0.37	28	57.99

Table 4. Figures of merit of aliasing for the set of six test images directly subsampled by a factor 5 without the pre-filtering and then interpolated to the original pixel dimensions.

Test images	Srin%	PE	UPP%
Livorno	21.55	100	19.60
San Rossore	5.71	77	43.24
Pisa airport	17.34	99	22.17
Tuscany 1	7.67	92	31.76
Basilicata 1	6.94	103	24.27
Basilicata 2	7.26	85	15.81

Table 5. Percentage of the figures of merit evaluated for the prefiltered and downsampled images with respect to those of the image downsampled without instrument pre-filtering

Test mages	Srin % ⇑	PE % ⇑	UPP% ⇓
Livorno	4.01	25.00	320.51
San Rossore	5.50	19.48	211.37
Pisa airport	5.25	21.21	312.67
Tuscany 1	5.33	20.65	262.09
Basilicata 1	5.71	24.27	301.98
Basilicata 2	5.14	32.94	366.79

To give an idea of the level of aliasing in these tests, i.e. to find out if the score indexes are high or low in absolute terms, direct decimation of the original images of a factor five was considered and score indexes computed. Table 4 presents the results in this case that is obviously the worst. Indexes reveals that aliasing is now significant.

In Table 5, the ratio between the figures of merit, evaluated with system pre-filtering are shown. The resulting ratios are an index of the aliasing decrease due to the system pre-filtering and give an idea of the amount of aliasing relatively to the worst case.

7 ALIASING MITIGATION

Aliasing mitigation is obtained by two powerful filtering schemes recently proposed in the literature.

The first scheme is a multi-resolution based filter that exploits the advantages of ratio Laplacian pyramid (RLP) to match the signal-dependent nature of noise (Aiazzi 1998). Local statistics filtering is applied to the different spatial resolutions of the RLP of a noisy image. For natural scenes, each pyramid layer is characterized by a SNR increasing as resolution decreases. Thus, each filter may be adjusted to achieve adaptivity also across scales. In addition, the estimation of the local statistics driving the filter is more accurate thanks to the multi-resolution framework.

The second algorithm is of *fuzzy* nature. Space-varying linear MMSE estimation is stated as a problem of *matching pursuits*, in which the estimator is obtained as an expansion in series of a finite number of *prototype* estimators (Aiazzi 2001), fitting the spatial features of the different statistical classes encountered. Such estimators are calculated in a fuzzy fashion through an automatic training procedure. The space-varying coefficients of the expansion are stated as degrees of fuzzy membership of a pixel to each of the estimators. ``A priori" knowledge on the noise variance is not required, nor a particular signal model is assumed. The image of Fig. 8a is obtained by processing the image of Fig. 7a by means of RLP filter. Some reduction of aliasing is visible on linear features. This reduction is more appreciable by observing Fig. 8b; in this last the difference between Fig. 8a and the *not-aliased* image is reported.

Correspondingly Fig. 9a reports the results obtained by applying the fuzzy filtering scheme to Fig. 7a while Fig. 9b shows the difference between Fig. 9a and the *not-aliased* image. A comparison between Figs. 8 and 9 shows that both filters are effective, being the fuzzy filter a little bit sharper on edges. In particular we can notice the aliasing patterns on the left side of the image and on the runway. The proposed filters are particularly efficient on these features that are cleaned without apparently loosing their sharpness.The substantial equivalence of the two filters is confirmed by tables 6 and 7, where the score indexes have been measured on the

filtered images. Close to each parameter its variation with respect to its value measured on the *aliased* image is reported. Again all the score indexes show the same trend; performance always improves after filtering. The fuzzy filtering scheme seems to work better on contours as assessed by the peak error. The increase in UPP is also noteworthy: it is negligible on images containing large homogeneous areas while is appreciable on all the other images.

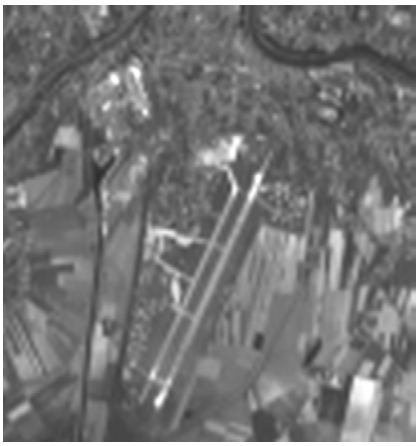

Figure 7. (a-top) Image decimated and interpolated by 5; (b-bottom) difference between image 7a and *not-aliased* image

Table 6. Figures of merit of aliasing for the set of six aliased images after Pyramid filtering

Aliased 450 nm	Srin %	ΔSRin %	PE	ΔPE %	UPP %	ΔUPP %
Livorno	0.62	27.9	20	20.0	68.1	8.4
San Rossore	0.25	21.9	10	33.3	93.7	2.5
Pisa air.	0.60	34.1	13	38.1	75.0	8.2
Tuscany	0.31	26.2	17	10.5	87.0	4.6
Basil. 1	0.27	32.5	22	12.0	79.7	8.7
Basil. 2	0.26	31.6	23	17.9	65.2	12.4

Table 7. Figures of merit of aliasing for the set of six aliased images after processing with Fuzzy filter

Aliased 450 nm	Srin %	ΔSRin %	PE	ΔPE %	UPP %	ΔUPP %
Livorno	0.59	31.4	18	8.0	68.7	9.4
SanRoss.	0.26	18.8	8	46.7	93.7	2.5
Pisaair.	0.61	33.0	14	33.3	75.0	8.2
Tuscany	0.30	28.6	13	31.6	86.9	4.4
Basil. 1	0.26	35.0	19	24.0	79.9	9.0
Basil. 2	0.25	34.2	16	42.9	65.4	12.8

8 CONCLUDING REMARKS

A general procedure to evaluate aliasing utilizing simulated images has been proposed. A model for PRISM hyper-spectral sensor has been developed and used to produce simulated PRISM images that have been analyzed, in order to verify and assess aliasing effects by means of proper score indexes and visual inspection. The adopted score indexes showed that aliasing phenomenon in the simulated images is moderate. Some visual degradations appears only on significant linear features, on edges and on high texture areas. Adaptive filtering based on multi-resolution and on fuzzy schemes can significantly contribute to mitigate aliasing effects with negligible penalty on spatial resolution.

REFERENCES

Aiazzi B., Alparone L., Baronti S. & Borri G. 1998 Pyramid-Based Multi-resolution Adaptive Filters for Additive and Multiplicative Image Noise, *IEEE Trans. Circuits and Systems-II:Analog and Digital Signal Processing*, Vol. 45(No. 8):1092-1096.

Aiazzi B., Alparone L. & Baronti S. 1998 Multi-Resolution Local-Statistics Speckle Filtering Based on a Ratio Laplacian Pyramid, *IEEE Trans. Geoscience and Remote Sensing*, Vol. 36(No. 5):1466-14761.

Aiazzi B., Alparone L., Baronti S. & Bianchini M. 2001 Blind estimation of interferometric SAR phase images through fuzzy matching-pursuits, in Proc. SPIE Vol. 4541:59-69.

Cooke B.J, Laubscher B. E. Borel C.C, Lomheim T.S. & Klein C. F. 1996 Methodology for rapid infrared multispectral, electro-optical imaging system performance analysis and synthesis; *in Proc. SPIE* Vol. 2743:52-86.

Goodman J. W. 1996 *Introduction to Fourier Optics*, McGraw-Hill

Jacobs E. L. & Edwards T. C. 1999 Sampling criteria for sensor simulation *Optical Engineering,* Vol. 38(No. 5):827-835.

Nyquist H. 1928 Certain topics on telegraph transmission theory, *tr. of American Institute of Electrical Engineers*, Vol. 47:617-644.

Oppenheim A.V., Schafer R.W. 1989 *Discrete-time signal processing*. Prentice-Hall.

Park S. K. & Rahman Z. 1999 Fidelity Analysis of sampled imaging system, *Optical Engineering*, Vol. 38 (No. 5):786-800.

Pratt W. K. 1978. *Digital Image Processing*. John Wiley & Sons USA.

Shannon C.E, 1949 Communication in the presence of Noise, *Proc. Of the I.R.E.*, Vol. 37:10-21.
Vollmerhausen R. H., Driggers R. G. & O'Kane, B 1999 Influence of sampling on target recognition and identification *Optical Eng*ineering, Vol. 38(No. 5):763-772.
Vollmerhausen R. H. & Driggers R.G. 2000 *Analysis of sampled Imaging System*s, SPIE PRESS Bellingham, Washington USA.
ESA ESTEC Final Report of Estec contract 13016/98/NL/GD, 1999 *Phase A study for the Land Surface Process and interactions mission*, Alcatel Space Industries.

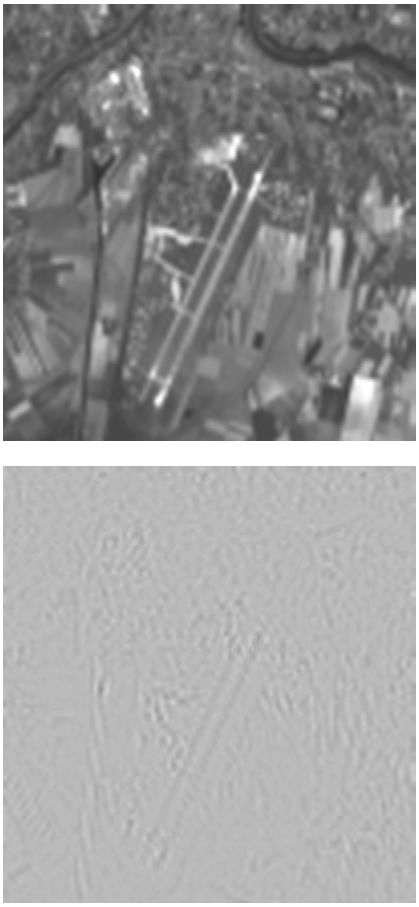

Figure 8. (a-top) Image of Figure 9a filtered with RLP; (b-bottom) difference between image 10a and *not-aliased* image

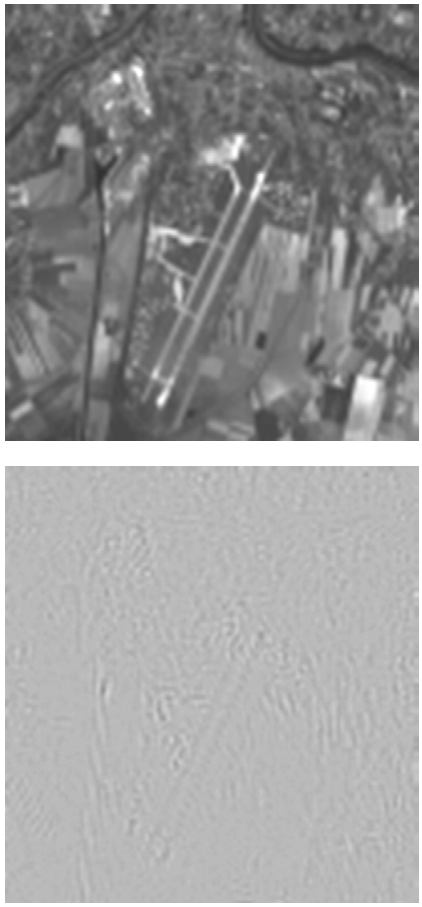

Figure 9. (a-top) Image of Figure 9a fuzzy filtered; (b-bottom) difference between image 11a and *not-aliased* image